Design and expression of human α7 nicotinic acetylcholine receptor extracellular domain mutants with enhanced solubility and ligand-binding properties

ARTICLE *in* BIOCHIMICA ET BIOPHYSICA ACTA · DECEMBER 2008

Impact Factor: 4.66 · DOI: 10.1016/j.bbapap.2008.11.002 · Source: PubMed

5 AUTHORS, INCLUDING:

Paraskevi Zisimopoulou
Hellenic Pasteur Institute, Athens, Greece
31 PUBLICATIONS **239** CITATIONS
SEE PROFILE

Elias Eliopoulos
Agricultural University of Athens
97 PUBLICATIONS **2,454** CITATIONS
SEE PROFILE

Konstantinos Poulas
University of Patras
78 PUBLICATIONS **664** CITATIONS
SEE PROFILE

Socrates J Tzartos
Hellenic Pasteur Institute (HPI)
260 PUBLICATIONS **6,598** CITATIONS
SEE PROFILE

Biochimica et Biophysica Acta 1794 (2009) 355–366

Contents lists available at ScienceDirect

Biochimica et Biophysica Acta

journal homepage: www.elsevier.com/locate/bbapap

Design and expression of human α7 nicotinic acetylcholine receptor extracellular domain mutants with enhanced solubility and ligand-binding properties

Marios Zouridakis [a,b,1], Paraskevi Zisimopoulou [a,1], Elias Eliopoulos [c], Konstantinos Poulas [b], Socrates J. Tzartos [a,b,*]

[a] Department of Biochemistry, Hellenic Pasteur Institute, 127, V. Sofias Ave., GR11521, Athens, Greece
[b] Department of Pharmacy, University of Patras, Rio, GR26500, Patras, Greece
[c] Department of Agricultural Biotechnology, Agricultural University of Athens, 75, Iera Odos, Votanikos, GR11855, Athens, Greece

ARTICLE INFO

Article history:
Received 14 September 2008
Received in revised form 2 November 2008
Accepted 4 November 2008
Available online 19 November 2008

Keywords:
Human α7 nicotinic acetylcholine receptor extracellular domain
3D model
Circular dichroism spectroscopy
Ligand-binding
Dynamic light scattering
Electron microscopy

ABSTRACT

In order to facilitate structural studies of the extracellular domain (ECD) of human α7 nicotinic acetylcholine receptor (nAChR), we designed several mutants, since the wild-type-ECD forms large oligomers and microaggregates, and expressed them in the yeast *Pichia pastoris*. Mutant design was based on a 3D model of human α7-nAChR-ECD, constructed using as templates the X-ray crystal structure of the homologous acetylcholine-binding protein (AChBP) and the electron microscopy structure of the *Torpedo* α-nAChR-ECD. At least one mutant, mut10, carrying six single-point mutations (Phe3Tyr, Val69Thr, Cys116Ser, Ile165Thr, Val177Thr, Phe187Tyr) and the replacement of its Cys-loop with the corresponding and more hydrophilic AChBP Cys-loop, was expressed with a 4-fold higher expression yield (1.2 mg/L) than the wild-type α7-ECD, existing exclusively as a soluble oligomeric, probably pentameric, form, at concentrations up to at least 10 mg/mL, as judged by gel filtration and dynamic light scattering. This mutant displayed a significantly improved ^{125}I-α-bungarotoxin-binding affinity (K_d=24 nM) compared to the wild-type-ECD (K_d=70 nM), the binding being inhibited by unlabelled α-bungarotoxin, D-tubocurarine or nicotine (K_i of 21.5 nM, 127 μM and 17.5 mM, respectively). Circular dichroism studies of mut10 revealed (a) a similar secondary structure composition (~5% α-helix, ~45% β-sheet) to that of the AChBP, *Torpedo* α-nAChR-ECD, and mouse α1-nAChR-ECD, (b) a well-defined tertiary structure and (c) binding of small cholinergic ligands at micromolar concentrations. Furthermore, electron microscopy showed well-assembled, probably pentameric, particles of mut10. Finally, since deglycosylation did not alter its solubility or ligand-binding properties, mut10, in either its glycosylated or deglycosylated form, is a promising α7-ECD mutant for structural studies, useful for the rational drug design to treat α7-nAChR-related diseases.

1. Introduction

Nicotinic acetylcholine receptors (nAChRs) belong to the superfamily of ligand-gated ion channels (LGICs), which also includes the 5-HT$_3$, glycine, GABA$_A$ and GABA$_C$ receptors [1–3]. The nAChR is made up of five subunits arranged with fivefold or pseudo-fivefold symmetry around a central pore. Each nAChR subunit consists of an N-terminal extracellular domain (ECD) containing the characteristic Cys-loop, four membrane-spanning α-helices, a large cytoplasmic loop and a small C-terminal extracellular domain [4]. The five subunits can either be homologous, e.g. $\alpha 1_{(2)}\beta 1\gamma\delta$ in the heteropentameric muscle-type *Torpedo* nAChR, or identical, as in the human homopentameric neuronal α7-nAChR [5].

Regarding the atomic structure of nAChR, four major breakthroughs have been achieved over the last few years. The first was the X-ray crystal structure of the molluscan homopentameric acetylcholine-binding protein (AChBP) and its complexes with various ligands (agonists and antagonists) [6–13]. Since the AChBP shows high homology with the nAChR α-ECDs, especially the human α7-ECD, this study for the first time revealed the nature of the nAChR ligand-binding site. The second was the 4 Å electron microscopy (EM) structure of the *Torpedo* nAChR, which showed the architecture of the muscle-type nAChR subunits and the fivefold symmetry of the receptor [14]. However, given the relatively low-resolution, no atomic details for the ligand-binding site could be observed. The third was the

Abbreviations: α-bgtx, α-bungarotoxin; α7-dm-ECD, double mutant of the α7-ECD; α7-wt-ECD, wild-type of the α7-ECD; ACh, acetylcholine; AChBP, acetylcholine-binding protein; BSA, bovine serum albumin; CCh, carbamylcholine; CD, circular dichroism; DLS, dynamic light scattering; ECD, extracellular domain; EM, electron microscopy; LGICs, ligand-gated ion channels; Ls-AChBP, *Lymnaea stagnalis* acetylcholine-binding protein; mAb, monoclonal antibody; nAChR, nicotinic acetylcholine receptor; nAChR-ECD, extracellular domain of the nicotinic acetylcholine receptor; PB, phosphate buffer

* Corresponding author. Department of Biochemistry, Hellenic Pasteur Institute, 127, V. Sofias Ave., GR11521, Athens, Greece. Tel.: +30 2106478844; fax: +30 2106478842.
E-mail addresses: tzartos@pasteur.gr, tzartos@upatras.gr (S.J. Tzartos).

[1] These authors contributed equally to this work.

1570-9639/$ – see front matter © 2008 Elsevier B.V. All rights reserved.
doi:10.1016/j.bbapap.2008.11.002

high-resolution X-ray crystal structure of the mouse muscle α1-nAChR-ECD bound to the nAChR antagonist α-bungarotoxin (α-bgtx) [15], which revealed atomic details for several key functional elements of the nAChR, such as the main immunogenic region (MIR), against which a large number of anti-nAChR antibodies are directed in the disease myasthenia gravis [16], loops A, B and C, which form the "principal side" of the nAChR ligand-binding pocket, and the signature Cys-loop. The structure of the monomeric α1-ECD also revealed the ordering of the carbohydrate chain linked to Asn141 of the α1-ECD and its crucial role in α-bgtx-binding. However, this study did not elucidate the structure of a complete nAChR ligand-binding site, due to the absence of an adjacent γ(ε) or δ-ECD. Finally, the fourth breakthrough was the high-resolution X-ray crystal structure of a prokaryotic LGIC (ELIC) from the bacterium *Erwinia chryssantemi*, considered to be the ancestor of eukaryotic LGICs [17]. The structure of ELIC revealed similarities with nAChR regarding the overall architecture of its ECD and transmembrane domain and some differences, such as the lack of an N-terminal α-helix, the Cys-loop and the cytoplasmic region. However, the structure of ELIC represents the minimal core structure of the nAChR and other members of the LGIC superfamily.

Despite the significant progress, it still remains essential to obtain a high-resolution structure of a pentameric nAChR in order to define the details of the ligand-binding pockets. The neuronal α7-nAChR is a good candidate for achieving this goal, since it is a homopentamer and forms five ligand-binding sites between its ECDs. Apart from serving as a model for the pentameric nAChR, the elucidation of the structure of the α7-nAChR at high resolution is also required for the rational design of drugs for the treatment of neurological diseases and disorders related to this receptor (reviewed in [18]). Furthermore, since the ECD of the α7-nAChR subunit is of pharmacological interest and since it lacks the large hydrophobic transmembrane domains of the intact receptor, it seems more realistic to perform high-resolution structural studies on this domain.

We had previously expressed the wild-type human α7-ECD (α7-wt-ECD) and a double mutant (α7-dm-ECD) in the yeast *P. pastoris* with the aim of obtaining sufficient material for detailed structural analysis [19]. The α7-wt-ECD was expressed in the form of large oligomers and microaggregates, whereas the α7-dm-ECD, in which Cys116 was mutated to Ser and the Cys-loop (Cys128–Cys142) was replaced by the corresponding and more hydrophilic loop region of *Lymnaea stagnalis* AChBP (Ls-AChBP), was more soluble and had a higher ^{125}I-α-bgtx-binding affinity [19]. However, this mutant was still aggregation-prone to some extent and thus unsuitable for crystallization trials. In the current study, we based on the 3D model of the human α7-ECD, constructed using the X-ray crystal structure of Ls-AChBP [6] and the EM structure of the *Torpedo* α-nAChR-ECD [14] as templates, and mutated several amino acid residues in order to enhance the solubility and assembly of the expressed α7-ECDs into stable pentamers. We describe here mostly a novel α7-ECD mutant, mut10, with significantly enhanced solubility (soluble up to at least 10 mg/mL, as usually required for structural studies) and ligand-binding properties compared to the wild-type and other mutants in both its glycosylated and deglycosylated forms. Moreover, evidence for its correct folding and assembly, probably as a pentamer, as well as the greatly improved expression yield, render it a promising starting material for structural studies.

2. Materials and methods

2.1. Construction of a three-dimensional model of the human α7-nAChR-ECD

The sequences of the human α7-nAChR-ECD and *Torpedo* α-nAChR-ECD were aligned using the ClustalW program [20] (Fig. 1). 3D models of the human α7-ECD were created with MODELLER v8.2 [21], using the *Torpedo* α-ECD (pdb code 2BG9) [14]

```
                10        20        30        40        50
                |         |         |         |         |
hα7wt       GEFQRKLYKELVKNYNPLERPVANDSQPLTVYFSLSLLQIMDVDEKNQVLTTNIWLQMSW 60
hα7mut10    GEYQRKLYKELVKNYNPLERPVANDSQPLTVYFSLSLLQIMDVDEKNQVLTTNIWLQMSW 60
Tα          SEHETRLVANLLENYNKVIRPVEHHTHFVDITVGLQLIQLINVDEVNQIVETNVRLRQQW 60
mα1         SEHETRLVAKLFEDYSSVVRPVEDHREIVQVTVGLQLIQLINVDEVNQIVTTNVRLKQQW 60
Ls-AChBP    -LDRADILYNIRQTSRPDVIPTQRDR-PVAVSVSLKFINILEVNEITNEVDVVFWQQTTW 58
               .  :  :: :       *.  .   : : ..*.:::::::*:* .: : .  .  :  *

                70        80        90        100       110
                |         |         |         |         |
hα7wt       TDHYLQWNVSEYPGVKTVRFPDGQIWKPDILLYNSADERFDATFHTNVLVNSSGHCQYLP 120
hα7mut10    TDHYLQWNTSEYPGVKTVRFPDGQIWKPDILLYNSADERFDATFHTNVLVNSSGHSQYLP 120
Tα          IDVRLRWNPADYGGIKKIRLPSDDVWLPDLVLYNNADGDFAIVHMTKLLLDYTGKIMWTP 120
mα1         VDYNLKWNPDDYGGVKKIHIPSEKIWRPDVVLYNNADGDFAIVKFTKVLLDYTGHITWTP 120
Ls-AChBP    SDRTLAWNSSHSP--DQVSVPISSLWVPDLAAYNAISKPEVLTPQLARVVS-DGEVLYMP 115
             *  * **  .    . : .*  .:* **:  **  .     .     ::.  *.  : *

                130       140       150       160       170
                |         |         |         |         |
hα7wt       PGIFKSSCYIDVRWFPFDVQHCKLKFGSWSYGG--WSLDLQMQEADISGYIPN-GEWDLV 177
hα7mut10    PGIFKSSCDVSG-VDTESGATCKLKFGSWSYGG--WSLDLQMQEADTSGYIPN-GEWDLT 176
Tα          PAIFKSYCEIIVTHFPFDQQNCTMKLGIWTYDGTKVSISPESDRPDLSTFMES-GEWVMK 179
mα1         PAIFKSYCEIIVTHFPFDEQNCSMKLGTWTYDGSVVAINPESDQPDLSNFMES-GEWVIK 179
Ls-AChBP    SIRQRFSCDVSG-VDTESGATCRIKIGSWTHHSREISVDPTTENSDDSEYFSQYSRFEIL 174
            .   :  * :     . .   * :*:* *:: .   ::.   :..* * :: . ..: :

                180       190       200
                |         |         |
hα7wt       GIPGKRSERFYECC-KEPYPDVTFTVTMRRRT----- 208
hα7mut10    GIPGKRSERYYECC-KEPYPDVTFTVTMRRRT----- 207
Tα          DYRGWKHWVYYTCCPDTPYLDITYHFIMQRI------ 210
mα1         EARGWKHWVFYSCCPTTPYLDITYHFVMQRL------ 210
Ls-AChBP    DVTQKKNSVTYSCC-PEAYEDVEVSLNFRKKGRSEIL 210
                :    * **   .* *:   . :::
```

Fig. 1. Sequence alignment of nAChR-ECDs and the Ls-AChBP. All sequences are those of the mature proteins and were aligned with the ClustalW program on the EMBL-EBI server [20]. hα7wt, human α7-wt-ECD; hα7mut10, human α7 mut10 (Table 1); Tα, *Torpedo* α-ECD; mα1, mouse α1-ECD. The sequence identity of human α7-wt-ECD with the mouse α1-ECD or *Torpedo* α-ECD and with Ls-AChBP is ~39% and 25.5%, respectively, with sequence similarities of ~76% and 70%. Bold letters indicate the amino acid residues mutated in mut10. The recombinant α7-ECDs under study also contain a c-myc epitope followed by a 6XHis tag at the C-terminus.

as a monomer template and the Ls-AChBP (pdb code 1I9B) [6] as a pentamer template. The derived models were checked for folding and packing errors using the QUANTA-CHARMm program [22] to arrive at a combined model with no bad atom contacts and an optimal side-chain conformation. Mutants were constructed using QUANTA-CHARMm and checked for changes in the hydrophobic and electrostatic profile.

2.2. Plasmid construction and transformation of P. pastoris

The cDNAs for the human α7-wt-ECD and α7-dm-ECD, previously cloned into the pPICZαA expression vector [19], were subcloned into the pBlueScript vector after XhoI/XbaI digestion. The mutations were generated using the Gene Tailor Site-Directed Mutagenesis System (Invitrogen, USA), according to the manufacturer's instructions. The combinations of primers used to generate the mutations are given in Supplementary Table 1. When multiple mutations were required in one construct, they were generated sequentially. The sequence of all constructs was confirmed by automated DNA sequencing (Lark Technologies Inc., UK). cDNAs carrying the desired mutations were subcloned back into the pPICZaA vector using the same restriction sites. The pPICZαA constructs were electroporated into the methylotropic yeast *P. pastoris* strain X33 (Invitrogen) and transformed cells selected on YPDS plates (1% w/v yeast extract, 2% w/v peptone, 2% w/v dextrose and 1 M sorbitol) supplemented with zeocin (100 μg/mL) after 3 days of incubation at 30 °C.

2.3. Protein expression in P. pastoris

Single colonies of the transformants were initially inoculated into 5 mL of BMGY (1% w/v yeast extract, 2% w/v peptone, 100 mM phosphate buffer (PB), pH 7.0, 1.34% YNB, 4×10^{-5}% w/v biotin and 1% v/v glycerol). After 24 h at 30 °C, the cells were resuspended in 5 mL of BMMY (identical to BMGY, except that the glycerol was replaced by 0.5% methanol) to induce expression. After induction for 2 days with daily addition of methanol (0.5% v/v), the culture supernatants were tested for expression of α7-ECD (wild-type or mutants) by dot-blot analysis using anti-myc monoclonal antibody (mAb) as the primary antibody and horseradish peroxidase-conjugated polyclonal goat anti-mouse IgG antibodies (Dako, Denmark) as secondary antibody. The clones with the highest protein yield were used for large scale protein expression.

2.4. Protein purification

The culture supernatant containing the secreted α7-ECD (wild-type or mutant) was concentrated using a Minitan Ultrafiltration System (Millipore, USA) with a 10 kDa cut-off filter, dialyzed against 50 mM PB, 300 mM NaCl, 1 mM DTT, pH 8.0, and the recombinant protein purified by Ni^{2+}-NTA metal affinity chromatography (Qiagen, Germany), based on the C-terminal 6XHis tag. The recombinant α7-ECD was eluted in 150 mM imidazole, detected with a filter assay using labelled ^{125}I-α-bgtx (see Filter assay for ligand-binding to α7-ECDs), concentrated to 500 μL by centrifugation (2,500 g, 10 min, 4 °C) in Amicon tubes (Millipore, USA), filtered through a 0.22 μm filter (Nalgene, USA) and finally purified on an AKTA 90 FPLC purifier system (Amersham-Pharmacia, Germany), using a 24 mL Superose 12 column (Amersham-Pharmacia) and isocratic elution with 10 mM PB, 100 mM NaCl, pH 7.5, at a flow rate of 0.5 mL/min. Fractions of 0.5 mL were assayed for ^{125}I-α-bgtx-binding and analyzed by 12% SDS-PAGE followed by Coomassie Brilliant Blue staining or Western blot analysis using anti-myc mAb. Dot-blot analysis was also performed on the fractions using the same mAb and the protein concentration of each fraction was measured using the Bradford method (Bio-Rad, USA).

2.5. Filter assay for ligand-binding to α7-ECDs

Various amounts of purified α7-ECD (wild-type or mutants) were incubated for 3 h at 4 °C with 50,000 cpm of ^{125}I-α-bgtx (specific activity 200 cpm/fmol) in a final volume of 50 μL of PB-BSA buffer (10 mM PB, 0.2% BSA, pH 7.5). The samples were then diluted in 1 mL of 20 mM Tris, 0.05% Triton X-100, pH 7.5, and immediately filtered through a Whatman DE81 filter presoaked with the same buffer and the filter washed twice with 1 mL of buffer. Finally, the bound radioactivity was measured on a γ-counter. Non-specific binding was measured using samples not containing recombinant α7-ECD.

2.6. Scatchard plots

To determine the dissociation constant value (K_d) for each α7-ECD (wild-type and mutants) for ^{125}I-α-bgtx, Scatchard plot analysis was performed. Various concentrations (2.5–30 nM) of ^{125}I-α-bgtx were incubated for 3 h at 4 °C with 20 ng (~11 nM) of α7-ECD in a final volume of 50 μL of PB-BSA buffer, then bound ^{125}I-α-bgtx was measured as described in the section Filter assay for ligand-binding to α7-ECDs.

2.7. Competition experiments

Various amounts of unlabelled ligands [the antagonists α-bgtx and D-tubocurarine and the agonists nicotine, ACh and carbamycholine (CCh)] were added simultaneously with ^{125}I-α-bgtx (50,000 cpm) to 20 ng of purified α7-ECD (wild-type and mutants) in a final volume of 50 μL of PB-BSA and the mixture incubated for 3 h at 4 °C, then ECD-bound radioactivity was measured using the filter assay. The residual ^{125}I-α-bgtx-binding ability was determined as the percentage of the radioactivity bound in the presence of the unlabelled ligand divided by that in its absence. The K_i (inhibition constant) for each ligand was calculated using the Cheng–Prusoff equation: $K_i = IC_{50}/(1+[^{125}\text{I-}\alpha\text{-bgtx}]/K_d)$ [23], where IC_{50} is the concentration of the ligand causing 50% inhibition of ^{125}I-α-bgtx-binding, determined from the inhibition curve, [^{125}I-α-bgtx] the concentration of ^{125}I- α-bgtx used in the competition experiment and the K_d the dissociation constant for ^{125}I-α-bgtx, estimated from a Scatchard plot.

2.8. Circular dichroism studies

Circular dichroism (CD) spectra were recorded at 20 °C using a Jasco J-715 spectropolarimeter (Japan Spectroscopic Co.). The scan speed was set at 50 nm/min, the bandwidth at 1 nm, the response time at 2 s, the scan ranges at 190–260 nm (far-UV) and 250–320 nm (near-UV) and the resolution at 0.2 nm. All proteins were dissolved in 10 mM PB, 50 mM sodium fluoride, pH 7.5. The quartz cell path length was 1 or 10 mm for the far-UV or near-UV CD studies, respectively. Each spectrum represents the average of ten scans after subtraction of a buffer blank. The upper limit of the High Tension voltage was 600 V. Optical activity was expressed as the mean residue ellipticity {Θ} in degrees cm^2 $dmol^{-1}$, based on the mean residue mass of the α7-ECD (wild-type or mutant). Far-UV CD spectra were fitted using a database of 43 soluble proteins (SP43) of known 3D structure [24] and the secondary structure composition calculated using the programs CDSSTR, CONTINLL and SELCON3 included in the CDPro software [24]. For ligand-binding studies, 7 μM (~0.25 mg/mL) α7-ECD (or BSA or human muscle nAChR β1-ECD or γ-ECD as controls) was placed in a cuvette and scanned as a reference, then a final concentration of 10 μM α-bgtx or 10 μM or 1 mM ACh, CCh or nicotine was added, the mixture incubated at room temperature for 30 min, and the solution rescanned. The differential spectrum of α7-ECD was obtained by subtracting the CD spectrum of the ligand at the same concentration as in the complex from the CD spectrum of the complex (α7-ECD · ligand) before conversion of the ellipticity to mean residue ellipticity.

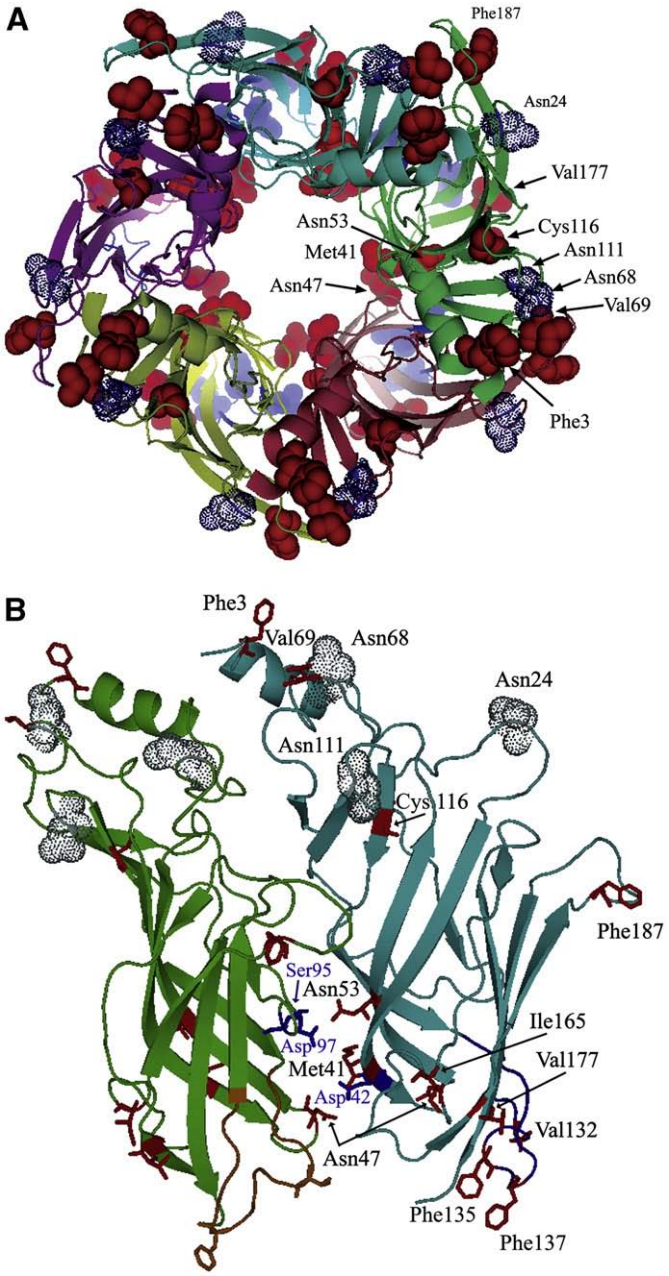

Fig. 2. Ribbon diagrams of the human nAChR α7-ECD model. (A) Top view of the homopentameric α7-ECD. Most of the mutated amino acid residues are shown in solid sphere representation. (B) Side-view of the α7-ECD homodimer. The side chains of all mutated residues are shown in solid stick representation. The side chains of Asp42, Ser95 and Asp97, at distances allowing potentially interaction with the interface-located residues Asn47, Asn53 and Met41, respectively, of the adjacent monomer are shown in blue. The three putative sites for N-linked glycosylation (Asn24, Asn68 and Asn111) are shown dotted. PYMOL was used for the preparation of the structure figures [35].

2.9. Dynamic light scattering studies

Dynamic light scattering (DLS) analysis of purified α7-ECD samples was performed using a Zetasizer NanoS Instrument (Malvern Instruments, UK) with a helium-neon laser providing 633 nm light and an output power of 4.0 mW. Samples were placed in a quartz cuvette and measurements made at 25 °C for an automatically determined time. The results were analyzed with DTS v.4.1 software. The estimated size for each α7-ECD sample is given as the mean hydrodynamic diameter (d.nm) of the particles calculated from the intensity of the scattered light. The molecular masses of the α7-ECDs were estimated based on those of a globular protein of the same size, and the polydispersity (Pd%) was calculated from the width (nm) of the peak of interest.

2.10. Electron microscopy studies

A colloidin film bearing copper grids (400 mesh; TAAB Laboratories Equipment Ltd.) was coated with a thin carbon layer and glow-discharged for 2 min prior to use. Purified α7-ECD (0.3 mg/mL) was added to the carbon-coated grids and embedded in 2% (w/v) uranyl acetate as negative stain. Images were taken at 40,000× magnification using a Philips 208 electron microscope operating at 80 kV.

2.11. In vitro deglycosylation of α7-ECD

Approximately 1.5 mg of purified α7-ECD was deglycosylated under native conditions by addition of 2,000 U of N-glycosidase F (PNGaseF) (New England Biolabs, USA) in 50 mM PB, pH 7.5 (final volume 500 μL) and incubation at 4 °C overnight. All experiments with deglycosylated α7-ECD were performed after removal of PNGaseF by gel filtration.

3. Results

3.1. Three-dimensional model of the human α7-ECD and initial mutant design

The constructed 3D model of the human α7-ECD (Fig. 2) revealed the spatial positions of the amino acid residues and aided in locating the interface residues between adjacent monomers. Since the α7-wt-ECD was expressed in the form of microaggregates and oligomers larger than the expected pentamers [19], we focused on locating hydrophobic amino acid residues of the pentameric α7-ECD model exposed to the environment that might account for the poor solubility of the wild-type protein. As shown in Fig. 2, several hydrophobic amino acid residues (Phe3, Val69, Val132, Phe135, Phe137, Ile165, Val177 and Phe187) were exposed in each α7-ECD monomer. These

Table 1
Description of the α7-ECDs studied

α7-ECD	Mutations	Aggregate/oligomer ratio[a]
wt	—	1:1.25
dm	Cys116Ser (β6 strand), AChBP-Cys-loop[b] [19]	1:2.50
mut1	Phe3Tyr (N-terminal α-helix)	1:2.00
mut2	Val69Thr (β2–β3 loop), Ile165Thr (β8–β9 loop), Val177Thr (β9 strand), Phe187Tyr (β9 strand)	1:4.00
mut3	Val132Thr (Cys-loop), Phe135Tyr (Cys-loop), Phe137Tyr (Cys-loop)	1:2.10
mut4	Phe3Tyr, Val69Thr, Val132Thr, Phe135Tyr, Phe137Tyr, Ile165Thr, Val177Thr, Phe187Tyr	1:4.30
mut5	Met41Lys (β1 strand)	1:1.10
mut6	Asn47Gln (β1–β2 loop), Asn53Gln (β2 strand)	1:1.25
mut7	Met41Lys, Asn47Gln, Asn53Gln	1:1.20
mut8	Phe3Tyr, Cys116Ser, AChBP-Cys-loop	1:3.00
mut9	Val69Thr, Cys116S, AChBP-Cys-loop, Ile165Thr, Val177Thr, Phe187Tyr	1:6.00
mut10	Phe3Tyr, Val69Thr, Cys116Ser, AChBP-Cys-loop, Ile165Thr, Val177Thr, Phe187Tyr	~0

The middle column shows the mutations introduced into the α7-ECD and their position in the secondary structure elements (in parentheses) of the α7-ECD model, as in [6] and [14]. mut4 contains all the mutations in mut1–3; mut7 contains all the mutations in mut5 and mut6; mut8 and mut9 contain, respectively, the same mutations as mut1 and mut2 inserted into the α7-dm-ECD; mut10 contains all mutations in mut8 and mut9.

[a] Aggregate/oligomer ratio of the protein calculated from gel filtration analysis of the expressed α7-ECDs.

[b] AChBP-Cys-loop: Replacement of the human α7-nAChR Cys-loop (Cys128–Cys142 loop; 13 amino acids) with the corresponding more hydrophilic loop of the Ls-AChBP (12 amino acids).

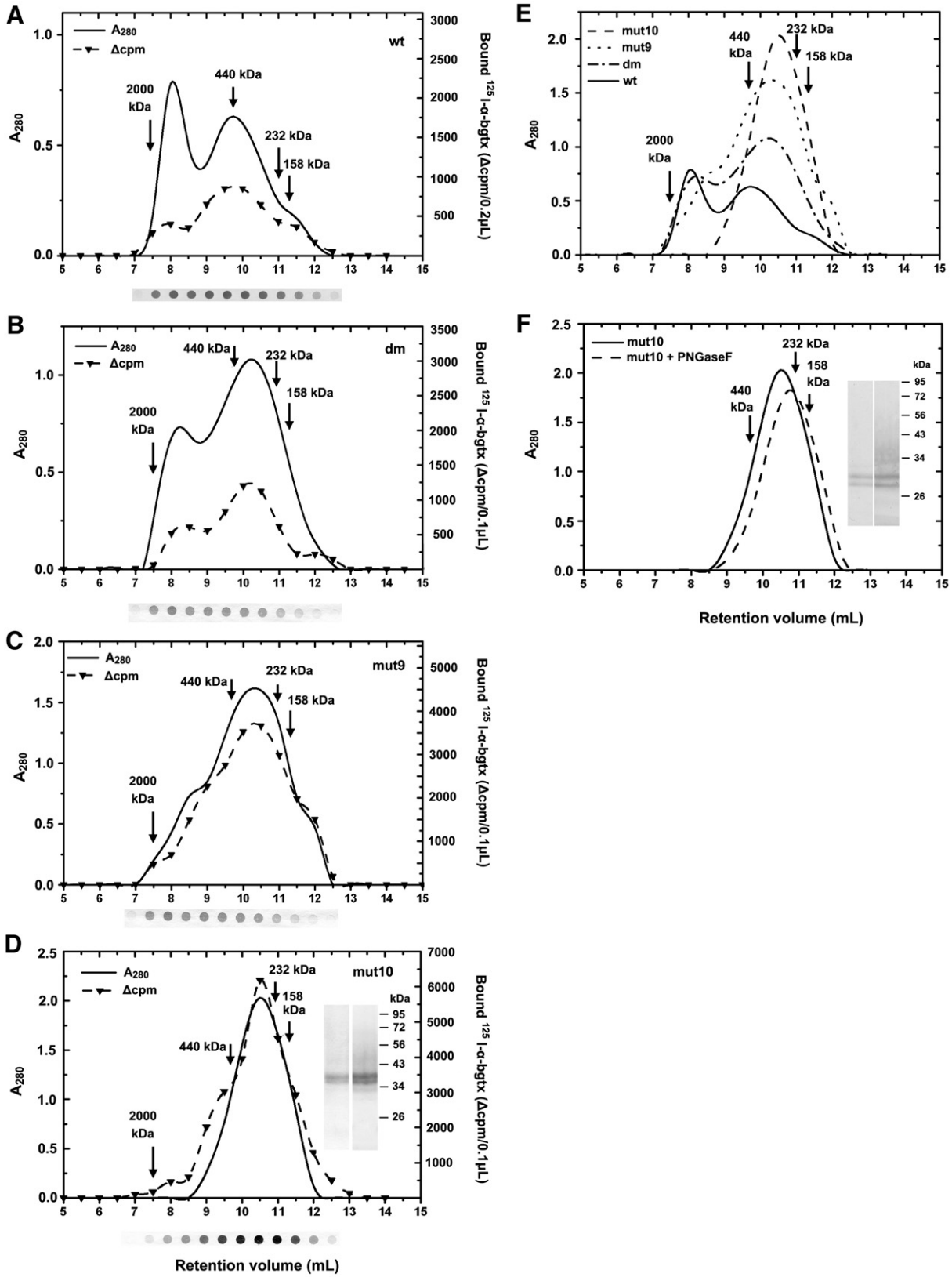

Fig. 3. Gel filtration analysis of expressed human α7-ECDs. (A–D): wt-ECD (A), dm-ECD (B), mut9 (C), and mut10 (D). The left y axis shows the protein absorbance at 280 nm (A_{280}) and the right y axis the bound ^{125}I-α-bgtx (Δcpm) in the filter assay. In the case of the wild-type, 0.2 μL of each gel filtration fraction was used in the filter assay, while, in all other cases, 0.1 μL was used. The solid lines represent the chromatographic profile of each α7-ECD and the dashed lines ^{125}I-α-bgtx-binding by the fractions. Dot-blots using anti-myc mAb for each fraction are shown below the chromatograms. The inset in (D) shows SDS-PAGE of a sample from the peak fraction of mut10. (Lane 1) Coomassie blue-stained; (Lane 2) Western blot with anti-myc mAb; the positions of the molecular mass standards are indicated on the right. (E) Superposition of the size exclusion chromatograms from (A–D) of α7-ECDs isolated from 1 L cultures of *P. pastoris*. (F) Gel filtration of glycosylated mut10 (solid line) and its deglycosylated form (dashed line) after treatment with PNGaseF. Inset to (F): as in (D), but using the peak fraction of the deglycosylated protein. In all panels, the arrows indicate the peaks of eluted protein markers of known molecular mass.

were mutated to more hydrophilic residues and four α7-ECD mutants were constructed, namely mut1, which contained a Phe3Tyr mutation in the N-terminal α-helix, mut2 with four mutated residues (Val69, Ile165, Val177 and Phe187) in the β-sandwich core, mut3 with three mutated residues (Val132, Phe135 and Phe137) in the Cys-loop region and mut4 containing all 8 of these point mutations (Table 1).

In addition, three residues (Met41, Asn47 and Asn53) located at distances from residues of adjacent monomers potentially allowing interaction were identified (Fig. 2B). These were also mutated to facilitate the possible formation of additional interactions with opposing residues of the adjacent monomer, which could enhance the assembly of the expressed ECDs into more stable pentamers. Thus, three new mutants, mut5–7, were constructed (Table 1). The replacement of Met41 by Lys in mut5 might lead to an electrostatic interaction with the 5 Å-distant Asp97 on the adjacent monomer (Fig. 2B). The replacement of both Asn residues in positions 47 and 53 by the larger Gln residue in mut6 could theoretically reduce the distances of 7 and 6 Å to, respectively, Asp42 and Ser95 of the adjacent monomer (Fig. 2B), and facilitate the formation of two hydrogen bonds. Mut7 contained all three of these mutations.

3.2. Gel filtration and dynamic light scattering analysis

The solubility and size of all α7-ECD mutants were studied by gel filtration and DLS. The previously expressed α7-wt-ECD and α7-dm-ECD [19] were included as references. As shown in Fig. 3A, the α7-wt-ECD was expressed in the form of high molecular mass aggregates and oligomers with a molecular mass of around 440 kDa. As expected [19], the α7-dm-ECD (Fig. 3B) was more soluble than the α7-wt-ECD, but still formed oligomers with a molecular mass higher than the value of ~200 kDa theoretically expected for glycosylated α7-ECD pentamers, and also formed microaggregates to some extent.

3.2.1. Mutants mut1–7

Mutants mut1–7 were also expressed in the form of oligomers and microaggregates. From all seven mutants, only those with mutations of the interface amino acid residues (mut5–7) exhibited an aggregate/oligomer ratio similar to that of the α7-wt-ECD (Table 1), and were, therefore, excluded from further analysis. Mutants mut1–3, in which the exposed hydrophobic residues were replaced by less hydrophobic ones, exhibited an oligomeric form with a molecular mass of around 440 kDa (data not shown), but the fraction of aggregated molecules was significantly decreased compared to that in the wild-type (Table 1). mut4 with all 8 mutations displayed oligomers with a molecular mass slightly less than 440 kDa (data not shown) and an aggregate/oligomer ratio even lower than that of the water-soluble α7-dm-ECD (Table 1). However, the oligomeric form of mut4 was still larger than that of α7-dm-ECD.

Table 2
Dynamic light scattering analysis of α7-ECDs

α7-ECD	Size (d.nm)	Estimated MW (kDa)	Pd (%)
wt	16.00±0.16	437	33.2±0.15
dm	13.85±0.11[a]	311	32.2±0.22
mut9	13.65±0.08[a,b]	301	31.5±0.17
mut10	12.50±0.12[a,b]	245	29.0±0.16
mut10+PNGaseF	11.50±0.15[a,b]	202	27.0±0.23

Measurements were performed using the peak gel filtration fraction of the oligomeric form of the expressed α7-ECDs (Fig. 3A–D, F). mut10+PNGaseF stands for deglycosylated mut10 and Pd for polydispersity. The data are the mean±S.D. values for five experiments.

[a] Statistically significantly different from the wild-type-ECD (one-way analysis of variance, F-Scheffé test, $p<0.01$).

[b] Statistically significantly different from the dm-ECD (one-way analysis of variance, F-Scheffé test, $p<0.01$).

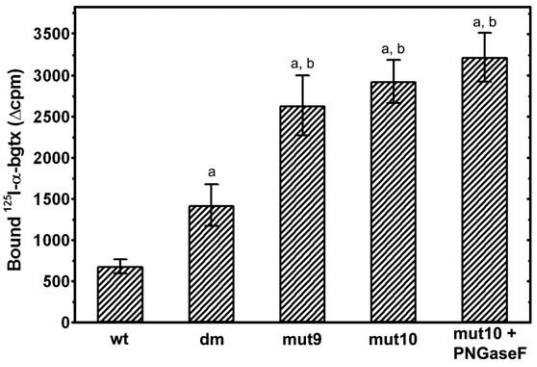

Fig. 4. Comparison of the ^{125}I-α-bgtx-binding ability of the α7-wt-ECD and the mutants. The same amount (20 ng) of the gel filtration peak fraction for each α7-ECD (wild-type and mutants) was incubated with 50,000 cpm of ^{125}I-α-bgtx and the bound radioactivity measured on a γ-counter (see Filter assay for ligand-binding to α7-ECDs). The column on the right is deglycosylated mut10, while the others are the glycosylated protein. The values are the mean and standard deviation (±S.D.) for at least 5 different experiments. [a]Statistically significantly different from the wild-type-ECD (one-way analysis of variance, F-Scheffé test, $p<0.01$). [b]Statistically significantly different from the dm-ECD (one-way analysis of variance, F-Scheffé test, $p<0.01$).

3.2.2. Mutants mut8–10 derived from combinations of the above mutations

Taking the above observations into account, we constructed and expressed three additional mutants, named mut8, mut9 and mut10 (Table 1). mut8 and mut9 contained the same mutation(s) as mut1 or mut2, respectively, superimposed on the α7-dm-ECD instead of the α7-wt-ECD, while mut10 contained all the mutations in mut8 and mut9. On gel filtration, mut9 (Fig. 3C) and mut10 (Fig. 3D) exhibited increased solubility compared to the α7-dm-ECD (Fig. 3B), whereas that of mut8 was similar to that of the α7-dm-ECD (data not shown). More precisely, the aggregated fraction was significantly decreased in mut9 compared to the α7-dm-ECD, while there were essentially no aggregates in mut10 (Fig. 3B–D; Table 1). Notably, the elution patterns of mut10 at concentrations up to at least 10 mg/mL were identical (data not shown). As shown in Table 2, the size of the oligomers estimated by DLS was significantly lower in mut10 compared to the α7-wt-ECD and α7-dm-ECD, corresponding to a molecular mass of 245 kDa, consistent with that suggested by gel filtration analysis (Fig. 3D). Furthermore, the polydispersity of the mut10 oligomers was significantly lower than that of the other ECDs (Table 2), as also indicated by the sharper peak in the chromatogram (Fig. 3E) and the

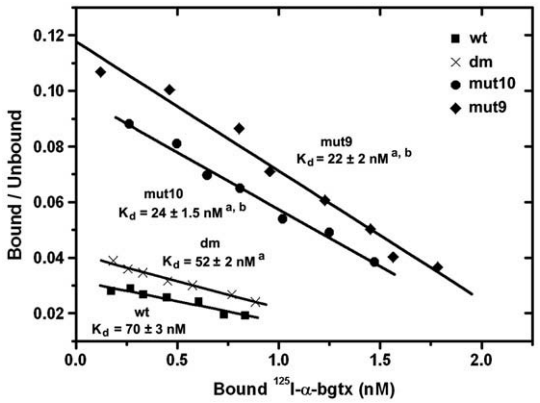

Fig. 5. Scatchard plots for ^{125}I-α-bgtx-binding to α7-ECDs. Representative experiment for α7-wt-ECD, α7-dm-ECD, mut9 and mut10. The mean K_d values (±S.D.) for these ECDs for at least 5 different experiments are shown in Table 3. [a]Statistically significantly different from the wild-type-ECD (one-way analysis of variance, F-Scheffé test, $p<0.01$). [b]Statistically significantly different from the dm-ECD (one-way analysis of variance, F-Scheffé test, $p<0.01$).

anti-myc dot-blots of the chromatography fractions (Fig. 3A–D). More precisely, in the case of mut10, the protein was only present as oligomers, in contrast to the other ECDs, which also contained aggregates. Finally, as it can be seen in Fig. 3E, which shows the superposition of the size exclusion chromatographs of α7-ECDs isolated from 1 L cultures of *P. pastoris* (Fig. 3A–D), the expression yield for mut9 and mut10 (1.2 mg/L for both) was 4 and 2-fold higher than that for the α7-wt-ECD (0.3 mg/L) or the α7-dm-ECD (0.6 mg/L), respectively.

3.3. Binding of ^{125}I-α-bgtx to α7-ECDs

The ability of mut9 and mut10 to bind ^{125}I-α-bgtx was tested in the filter assay and compared to that of the α7-wt-ECD and α7-dm-ECD. All gel filtration fractions of all four α7-ECDs exhibited ^{125}I-α-bgtx-binding ability (Fig. 3A–D). It is noteworthy that both mut9 and mut10 exhibited ~4-fold and ~2-fold higher toxin-binding ability than the α7-wt-ECD and α7-dm-ECD, respectively, as shown in Fig. 4, which represents the ^{125}I-α-bgtx-binding ability of equal amounts of each α7-ECD. This was confirmed by Scatchard plot analysis (Fig. 5), which showed that the K_d of these mutants for ^{125}I-α-bgtx (22 nM for mut9 and 24 nM for mut10) was ~2.5-fold lower than that of the α7-dm-ECD (52 nM) and ~3-fold lower than that of the α7-wt-ECD (70 nM). Mutants mut2–4 and mut8 also exhibited a lower K_d than the wild-type, but the difference was not as pronounced as with mut9 and mut10 (Table 3).

The binding of ^{125}I-α-bgtx to the α7-ECDs was found to be specific using different concentrations of unlabelled α-bgtx in competition assays. As shown in Fig. 6A, at the presence of a ~900-fold molar excess of non-labelled α-bgtx (10^{-5} M), non-specific binding to α7-ECDs (~11 nM) was in practice negligible. Moreover, unlabelled toxin inhibited the binding of ^{125}I-α-bgtx at nanomolar concentrations (Fig. 6A). The K_i values for unlabelled α-bgtx were consistent with the K_d values for ^{125}I-α-bgtx (Table 3) and confirmed the improved toxin-binding ability of mut9 and mut10 compared to the α7-wt-ECD and α7-dm-ECD.

3.4. Binding of small cholinergic ligands to α7-ECDs

As a further indication of correct folding and assembly, the ability of mut9 and mut10 to bind small cholinergic ligands was compared to that of the wild-type and double mutant. The binding of these ligands to α7-ECDs was assessed indirectly by their ability to inhibit the binding of ^{125}I-α-bgtx in co-incubation competition experiments. Both mut9 and mut10 were more capable than the α7-wt-ECD or the α7-dm-ECD of binding the antagonist D-tubocurarine (Fig. 6B), their K_i values being ~2-fold or ~1.5-fold lower than those for the α7-wt-ECD or α7-dm-ECD, respectively (Table 3). These mutants also bound the agonists nicotine (Fig. 6C, Table 3), ACh (data not shown) and CCh (data not shown) better than both the α7-wt-ECD and α7-dm-ECD, although millimolar concentrations of these ligands were needed to cause significant inhibition of ^{125}I-α-bgtx-binding. However, the K_i values of mut9 and mut10 for nicotine (16 and 17.5 mM), ACh and CCh (data not shown) were much lower than that of the negative control sodium chloride (78.5 mM) (Table 3), suggesting that the ability of these ligands to inhibit ^{125}I-α-bgtx-binding was specific, despite relatively weak.

3.5. Circular dichroism studies

The far-UV CD spectra of the α7-wt-ECD, α7-dm-ECD, mut9 and mut10 were all characteristic of β-sheet-rich proteins, as they showed a positive and negative Cotton effect in the 190–200 nm region and 200–220 nm region, respectively [25] (Fig. 7A). The CD spectra of all four α7-ECDs were almost superimposable over the whole far-UV range, with the spectrum of mut10 displaying some differences between 190–200 nm. Deconvolution of these spectra confirmed the similarity in the secondary structure composition of these four ECDs, characterized by the predominance of β-sheet structure (~45%) and a small α-helical content (~5%) (Table 4). However, the α-helical content of mut10 was slightly lower than that of the other ECDs (Table 4), which probably accounts for the differences observed in the 190–200 nm region (Fig. 7A). We also tested the effect of the antagonist α-bgtx and the agonists nicotine, ACh and CCh on the secondary structure of mut10 (the best mutant in terms of both solubility and ligand-binding properties) and found that this was not altered, since the presence of these ligands did not change the far-UV CD spectrum of mut10 (data not shown).

The near-UV CD spectra of these ECDs were all indicative of proteins with a well defined tertiary structure around their aromatic residues (Fig. 7B). The main feature of all the near-UV CD spectra was the pronounced strong negative peaks, of almost the same intensity, around 280 nm. However, the spectra of all three mutants displayed differences compared to that of the wild-type, especially around 255–270 nm and 275–285 nm, which are, respectively, regions where Phe and Tyr residues absorb. More specifically, α7-dm-ECD gave two distinct peaks at 277 and 282 nm, as did mut9 and mut10, whereas the wild-type gave only a peak at 280 nm. However, in the case of mut9 and mut10, the 282 nm peak was even more pronounced than with the α7-dm-ECD (and slightly red-shifted in the case of mut10), whereas the 280 nm peak was only more pronounced with mut10, although slightly red-shifted to 279 nm. These differences between the α7-dm-ECD and mut10 might be due to the replacement of two Phe residues by Tyr (Table 1). The peaks and shoulders observed in the

Table 3
Dissociation and inhibition constants for ligand-binding to α7-ECDs

α7-ECD	K_d (^{125}I-α-bgtx)	K_i (α-bgtx)	K_i (D-tubocurarine)	K_i (nicotine)	K_i (NaCl)
wt	70±3.0 nM	63.5±3.0 nM	233±22 μM	28.0±1.15 mM	
dm	52±2.0 nM[a**]	43.0±2.6 nM[a**]	188±14 μM[a**]	19.0±0.50 mM[a**]	
mut1	67±2.0 nM[b**]				
mut2	55±3.0 nM[a**,b*]				
mut3	54±4.0 nM[a**]				
mut4	48±3.5 nM[a**,b*]				
mut8	45±3.5 nM[a**,b**]				
mut9	22±2.0 nM[a**,b**]	19.0±1.7 nM[a**,b**]	139±8.0 μM[a**,b**]	16.0±1.20 mM[a**,b**]	
mut10	24±1.5 nM[a**,b**]	21.5±1.0 nM[a**,b**]	127±5.0 μM[a**,b**]	17.5±1.20 mM[a**,b*]	78.5±4.0 mM

The K_d values of each α7-ECD (wild-type and mutants) for ^{125}I-α-bgtx and the K_i values for the unlabelled ligands α-bgtx, D-tubocurarine or nicotine, were calculated as described in the sections Scatchard plots and Competition experiments, respectively. Non-specific binding to α7-ECD was determined from the K_i for sodium chloride (Fig. 6C). Mutants mut5-7 were not included in these studies, because they exhibited similar hydrophobicity with the α7-wt-ECD (Table 1). Empty cells denote no data. The K_i values for ACh and CCh were similar with these for nicotine (data not shown). The data are the mean±S.D. for at least five separate experiments.

[a] Statistically significantly different (one-way analysis of variance, F-Scheffé test) from the wild-type-ECD.

[b] Statistically significantly different (one-way analysis of variance, F-Scheffé test) from the dm-ECD.

* $p<0.05$.

** $p<0.01$.

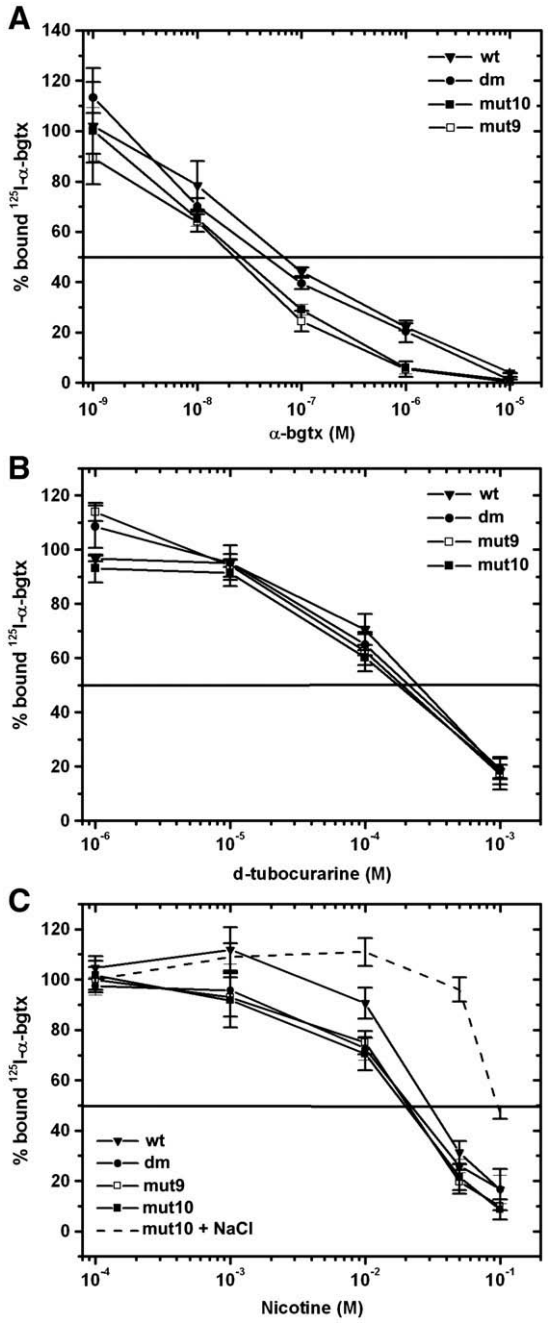

Fig. 6. Competition of ^{125}I-α-bgtx-binding to α7-ECDs by unlabelled ligands. Inhibition of ^{125}I-α-bgtx-binding to α7-ECDs was assessed by co-incubation competition experiments with unlabelled ligands, as described in the section Competition experiments. (A) α-bgtx, (B) D-tubocurarine, (C) nicotine. Non-specific inhibition was determined using sodium chloride (dashed curve in C). The ability of these ligands to inhibit ^{125}I-α-bgtx-binding to the α7-ECDs was determined by the IC_{50} value obtained from the curves and expressed as the K_i (values given in Table 3).

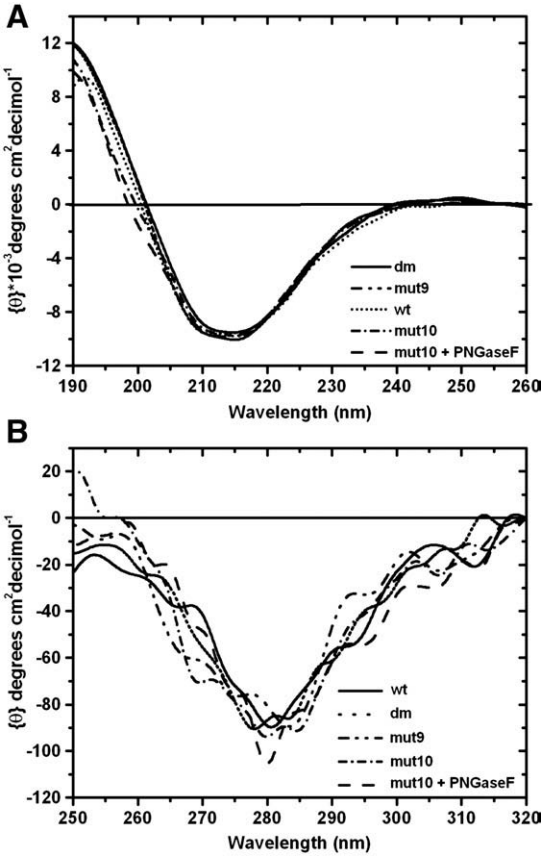

Fig. 7. CD spectra of α7-ECDs. (A) Far-UV. All the spectra are indicative of β-sheet-rich proteins and reveal a similar secondary structure composition of all the α7-ECDs tested (Table 4). (B) Near-UV. These spectra are indicative of proteins with a well-defined structure around their aromatic residues. The spectra of deglycosylated mut10 (mut10+PNGaseF) are also shown in (A) and (B).

255–275 nm region also showed a more pronounced negative ellipticity in all three mutants compared to the wild-type, the intensity increasing in the order α7-dm-ECD<mut9<mut10, reflecting the changes induced in the tertiary structure around Phe residues in these mutants.

In order to look for an effect of ligand-binding on the tertiary structure of mut10, we also performed near-UV CD studies in the presence of various ligands. The near-UV CD spectrum of 7 μM mut10 was significantly shifted upwards in the presence of the antagonist α-bgtx (Fig. 8A) or the small cholinergic agonists ACh (Fig. 8B) and CCh (Fig. 8C), implying that all three ligands bind. Interestingly, both ACh and CCh affected the CD spectrum even at low concentration values (μM), far lower than their effective concentrations in ^{125}I-α-bgtx competition experiments. To test whether the observed differences were due to specific binding or simply due to mutual perturbation of transitions in the two molecules (protein and ligand) brought into close proximity, 7 μM BSA was incubated with the same ligands and no significant differences were seen in its spectrum (Fig. 8D). As other negative controls, we also used the homologous human muscle nAChR β1-ECD and γ-ECD expressed in our laboratory [26]. Again, no difference was detected in their near-UV CD spectra as shown in the example of their incubation with CCh at the same concentration values used for mut10 (Fig. 8E, F). This is to be expected, as β1-ECD is not involved in ligand-binding sites, while γ-ECD alone does not form a ligand-binding site [14]. These results confirmed that the

Table 4
Secondary structure composition of human α7-ECDs, calculated from the far-UV CD spectra

α7-ECD	α-helix (%)	β-sheet (%)	β-turn (%)	Unordered (%)	NRMSD
wt	5.1	44.8	23.1	27.2	0.050
dm	4.4	45.0	23.8	29.0	0.070
mut9	4.7	43.8	22.9	27.1	0.079
mut10	3.8	44.9	24.4	26.7	0.066
mut10+PNGaseF	4.0	45.1	25.8	24.1	0.051

Optimal NRMSD (normalized root mean square deviation) values, issued from the comparison between experimental and back-calculated data (SP43 reference set), were obtained using the CDSSTR program [24], reflecting the accurate analysis of secondary structure (NRMSD<0.1) [25].

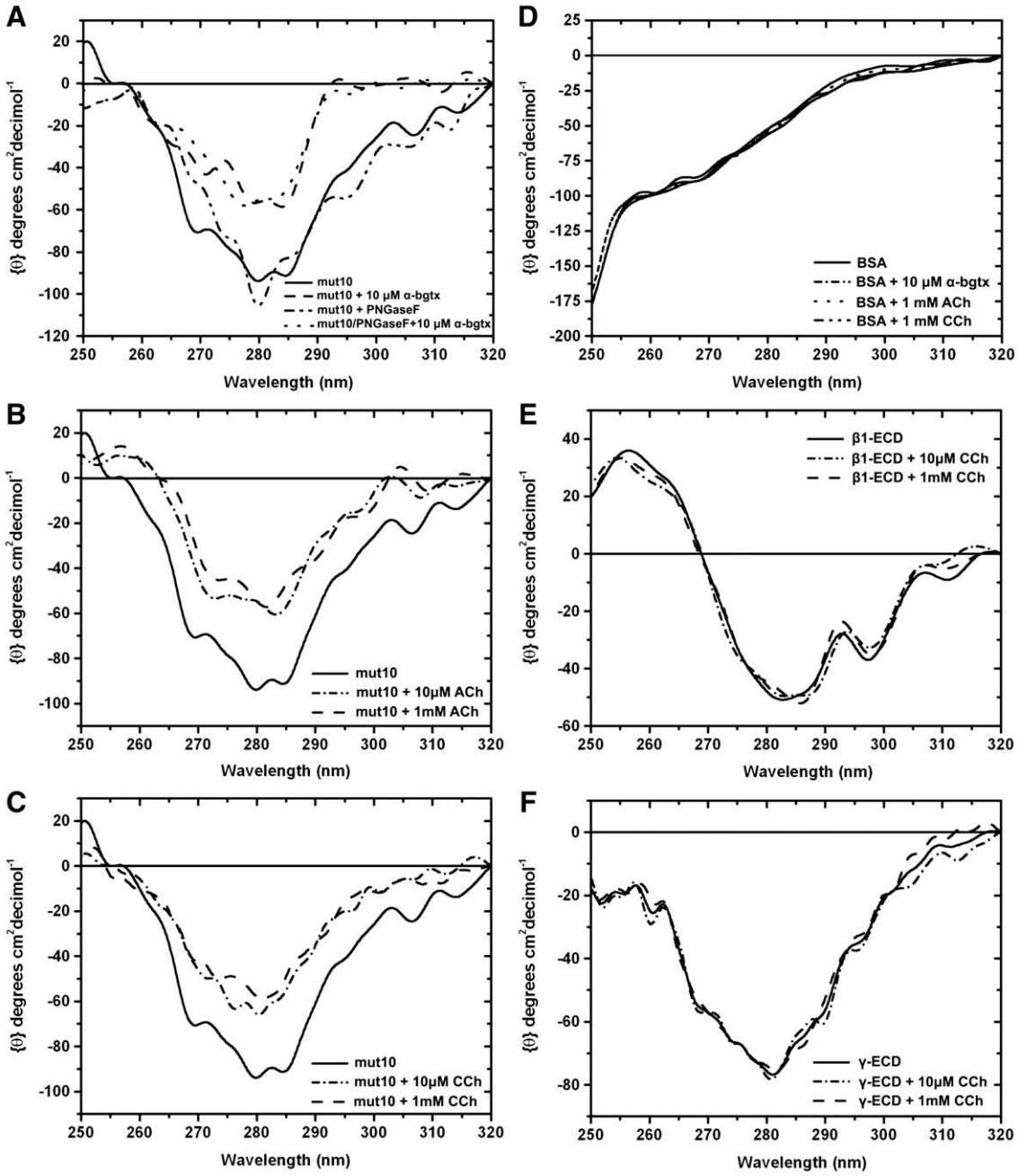

Fig. 8. Effect of ligand-binding on the tertiary structure of mut10. (A–C) Near-UV CD spectra of glycosylated mut10 (0.25 mg/mL; 7 μM) in the presence or absence of 10 μM α-bgtx (A) or 10 μM or 1 mM ACh (B) or CCh (C). The near-UV CD spectra of deglycosylated mut10 (+PNGaseF) in the presence or absence of 10 μM α-bgtx are also shown in (A). (D) Near-UV CD spectra of 7 μM BSA in the presence or absence 10 μM α-bgtx, 1 mM CCh or 1 mM ACh. (E, F) Near-UV CD spectra of 7 μM muscle nAChR β1-ECD (E) or γ-ECD (F) in the presence or absence of 10 μM or 1 mM CCh.

effect of ligand-binding on the near-UV CD spectrum of mut10 was specific.

3.6. Electron microscopy studies

Negative stain EM using the peak gel filtration fraction of mut10 revealed particles with similar shapes and sizes to the end-on views of EM images of the native *Torpedo* nAChR [27], muscle nAChR-ECDs [28] and the Ls-AChBP [29] (Fig. 9A). Moreover, these images clearly showed the existence of the characteristic central hole, as would be expected for a correctly assembled α7-ECD oligomer. Interestingly, well-assembled pentameric α7-ECDs with an average diameter of 10±0.5 nm could be observed within the population of complexes (Fig. 9B).

3.7. Effect of in vitro deglycosylation on mut10

Since protein glycosylation is often an obstacle in crystallization trials, we studied the effect of deglycosylation on mut10. As expected, this resulted in oligomers of lower molecular mass than the glycosylated form (Fig. 3F). SDS-PAGE analysis of the peak gel filtration fraction of deglycosylated mut10 revealed a double band of ~28 kDa (Fig. 3F), in contrast to the ~37 kDa double band seen with the glycosylated form (Fig. 3D). DLS analysis of the same gel filtration fraction confirmed the smaller size of deglycosylated mut10, the hydrodynamic diameter being 11.5 nm compared to the 12.5 nm of the glycosylated molecule (Table 2). The deglycosylated mut10 remained soluble and did not aggregate at concentrations as high as 10 mg/mL, which is a good starting point for crystallization trials.

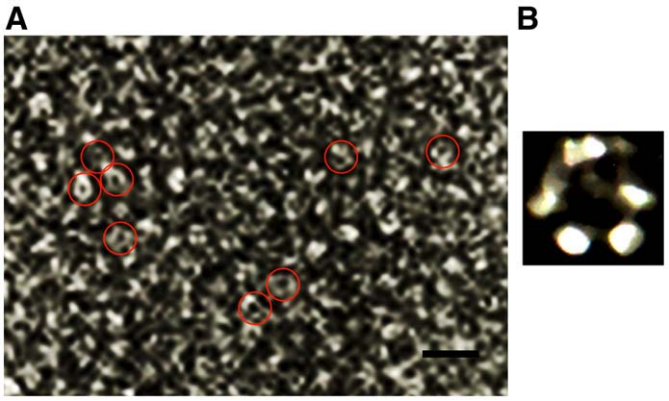

Fig. 9. Negative-stained electron microscopic images of mut10. (A) The red circles enclose end-on-views of α7-ECD oligomers forming the characteristic central hole, as expected for correctly assembled α7 molecules. (B) End-on-view of a characteristic α7-ECD oligomer selected from (A), confirming the existence of well-assembled homopentameric mut10 molecules. The scale bar in (A) is 20 nm.

The ^{125}I-α-bgtx-binding ability of deglycosylated mut10 did not differ significantly from that of the glycosylated (Fig. 4), also confirmed by the almost superimposable near-UV CD spectra of the α-bgtx complexes of glycosylated or deglycosylated mut10 (Fig. 8A). However, small differences were observed between the near-UV CD spectra of the free glycosylated and deglycosylated mut10 ECDs (Fig. 7B), probably due to the oligosaccharide chains present in the glycosylated protein. Analysis of the far-UV CD spectrum of deglycosylated mut10, which almost overlapped with the spectrum of the glycosylated form (Fig. 7A), revealed essentially the same secondary structure composition as the glycosylated molecule (Table 4).

4. Discussion

The high resolution X-ray crystal structures for AChBPs, the homologues of nAChR-ECDs, in their ligand-free and ligand-bound forms [6–13], the mouse nAChR α1-ECD bound to α-bgtx [15] and a prokaryotic LGIC [17], together with the 4 Å resolution EM structure of the *Torpedo* nAChR [14], have greatly advanced our knowledge of nAChR structure. However, despite the significant progress, the high-resolution structure of an intact human nAChR, or at least of intact extracellular domains is still needed to reveal the conformation of the complete ligand-binding site. The α7-nAChR-ECD is a good candidate for this purpose, as its expression has been shown to result in the formation of functional pentameric particles, although in minute amounts [30]. Elucidation of the structure of the human neuronal α7-ECD at high resolution, apart from serving as a model for the study of all other members of the LGIC superfamily, it is also of major pharmacological importance, since it would facilitate the rational design of drugs for treating α7-nAChR-related neurological diseases and disorders, such as Alzheimer's and Parkinson's diseases, schizophrenia, epilepsy, depression, and nicotine addiction (for review see [18]).

We have previously expressed the human α7-ECD in yeast *P. pastoris* [19] in order to obtain sufficient material for structural studies. The wild-type was expressed as microaggregates and large oligomers, whereas a double mutant (α7-dm-ECD), in which the Cys-loop region was replaced by the corresponding more hydrophilic loop region of Ls-AChBP and Cys116 was replaced by Ser, was expressed as more soluble oligomers, with a molecular mass close to that of the pentamer [19]. However, the formation of microaggregates, although at a lower extent than with the wild-type (Fig. 3A, B; Table 1), resulted in unsuccessful crystallization trials. Apparently, different or additional mutations were needed for a crystallisable α7-ECD.

In this study, we followed a mutagenesis strategy for human α7-ECD based on a 3D model (Fig. 2), constructed using as templates the X-ray crystal structure of Ls-AChBP [6] and the EM structure of the *Torpedo* α-nAChR-ECD [14]. The hydrophobic amino acids located on the surface of the molecule (Fig. 2) were replaced by less hydrophobic ones in mutants mut1–4 (Table 1). These mutants, with the exception of mut1, displayed significantly improved solubility and ^{125}I-α-bgtx-binding ability compared to the wild-type (Tables 1, 4). It should be noticed that mut3, with three residues of the Cys-loop mutated to less hydrophobic ones (Table 1), had a K_d for ^{125}I-α-bgtx (54 nM) very similar to that of the α7-dm-ECD (52 nM) (Table 3), in which the whole Cys-loop (13 amino acid residues) was replaced by the Ls-AChBP Cys-loop (12 residues) [19]. This implies that the improved ^{125}I-α-bgtx-binding ability of α7-dm-ECD compared to α7-wt-ECD (K_d=70 nM) may be mainly attributable to the replacement of these three residues. However, since mutants mut1–4 were still aggregation-prone to some extent and formed larger oligomers than a pentamer, we inserted these same mutations into the α7-dm-ECD, which was significantly more soluble than the α7-wt-ECD [19] (Fig. 3A, B). The derived mutants mut8–10 (Table 1) displayed lower K_d values for ^{125}I-α-bgtx compared to the wild-type, and mut9 and mut10 had K_d values even ~2.5-fold lower (22 and 24 nM, respectively) than that of the α7-dm-ECD (Table 3). The K_d values of mut9 and mut10 are closer to that of the native α7-nAChR (1.66 nM) [31], thus denoting an improved conformation of their ligand-binding sites, which probably results from an allosteric effect of the introduced mutations, as the mutated residues in mut9 and mut10 are away from these sites and are not known to contribute to their formation.

Mutants mut9 and mut10 were also the most soluble α7-ECDs, with aggregates being totally absent in mut10 (Table 1; Fig. 3C, D). The significantly increased solubility of these mutants may also account for their improved K_d values for ^{125}I-α-bgtx, because of a probably increased accessibility of the ligand-binding sites. The increase in the solubility of mut9 and mut10 was also accompanied by an improved expression yield (1.2 mg/L) compared to the wild-type-ECD (0.3 mg/L) and α7-dm-ECD (0.6 mg/L) (Fig. 3E). Furthermore, the mut10 oligomers were of lower molecular mass than those of the wild-type and other mutants, as judged by gel filtration (Fig. 3E) and DLS (Table 2). The hydrodynamic diameter of 12.5 nm calculated by DLS for the peak gel filtration fraction of glycosylated mut10 (Fig. 3D) may be higher than the ~8–9 nm expected for a pentameric nAChR [6, 14], but we must take into account the presence of additional residues (22 residues per monomer) in the amino sequence of mut10 (including the c-myc epitope and the 6XHis tag), which, depending on their conformation, could potentially increase the diameter of the expressed ECDs. In addition, the three putative sites of N-linked glycosylation (Asn24, 68 and 111) were located in our model on the top of the α7-ECD (Fig. 2) and the existence of carbohydrate chains with lengths possibly up to 2–3 nm, as observed in the structure of the mouse α1-ECD expressed in *P. pastoris* [15], might therefore also account for the observed difference. Nevertheless, the EM images of the same gel filtration fraction of mut10 revealed the existence of well-assembled pentamers with a diameter of 10±0.5 nm within the population of particles, forming the characteristic central pore between the constituent monomers (Fig. 9).

To address the question whether the introduced mutations altered the secondary or tertiary structure of the α7-ECD, far- and near-UV CD studies were performed. The far-UV CD spectra of mut10, mut9 and the previously studied α7-dm-ECD were very similar to that of the α7-wt-ECD (Fig. 7A), suggesting no effect on its secondary structure composition, calculated as ~45% β-sheet and ~5% α-helix

(Table 4). This is similar to the secondary structure composition of the Ls-AChBP (46% β-sheet; 9.5% α-helix) [6], mouse muscle α1-nAChR-ECD (47% β-sheet; 6% α-helix) [15], *Torpedo* α-nAChR-ECD (40% β-sheet; 5% α-helix) [14] and human muscle nAChR α1-, β1-, γ- and ε-ECDs (~40% β-sheet; ~5% α-helix) [32]. Furthermore, the near-UV CD spectra for mut10, mut9 and the α7-dm-ECD were indicative of proteins with a well defined tertiary structure. The differences between the near-UV CD spectra of the wild-type and mutants around the absorption wavelength of their aromatic residues (Fig. 7B) may be attributed (a) to the different oligomeric state among these ECDs, leading to the partial burial or exposure of aromatic residues, and/or (b) to the fact that aromatic residues were altered in the mutants, which may also have induced local conformational changes. Moreover, the changes in the tertiary structure of mut9 and mut10, as indicated by their near-UV CD spectra, must have led to an improved and probably near-native conformation, given their significantly enhanced ^{125}I-α-bgtx-binding ability (Table 3).

Further evidence for the correct folding of mut10 was the binding of small cholinergic ligands. Interestingly, mut10 (7 μM) bound ACh and CCh even in micromolar concentrations, as indicated by the significant shift upwards of its near-UV CD spectrum (Fig. 8B, C). This effect may have resulted from the direct interaction of the ligands with aromatic residues in the vicinity of the ligand-binding site [33], as well as from subsequent local conformational changes probably induced around aromatic residues at a distance from the binding-site [7–13]. In contrast, in ^{125}I-α-bgtx competition experiments, binding of small ligands to the α7-ECD (~11 nM) was only seen at a high ligand excess (millimolar concentrations), as in the example with nicotine (Table 3; Fig. 6C), suggesting that there is only weak stereochemical inhibition of binding of the larger ^{125}I-α-bgtx molecule to α7-ECD by small ligands. Nicotine and D-tubocurarine absorb excessively in the near-UV region (the latter also absorbs in the far-UV) and thus could not be used in CD studies.

Despite the successful crystallization of the glycosylated muscle α1-nAChR-ECD [15], glycosylated proteins are usually less useful for producing diffraction-quality crystals. In the case of the α1-ECD, the bound α-bgtx immobilized the carbohydrate groups, thus facilitating crystallization [15]. In contrast, α-bgtx-binding to the α7-ECD does not involve the carbohydrate [19], and therefore a water-soluble non-glycosylated form of α7-ECD is probably preferable for structural studies. Fortunately, mut10 was easily deglycosylated under native conditions using small amounts of PNGaseF without affecting its ligand-binding properties (Figs. 4, 8A) or secondary structure composition (Fig. 7A; Table 4). Additionally, the deglycosylated form was also soluble and did not aggregate even at concentrations up to 10 mg/mL (data not shown).

We based our selection of mutants on our model constructed on the basis of the EM structure of the *Torpedo* α-ECD and the X-ray structure of the Ls-AChBP, the only data available at the time. Recently, the published structure of the mouse α1-ECD was used to construct a new model for the human α7-ECD [34], which, when superimposed on that used in the current study, revealed the same location of the surface amino acid residues, but differences in the orientation of interface-located residues. This might explain the lack of success of mutants mut5–7 (Table 1), as the mutated interface-located residues were selected based on the model described in the current study.

In conclusion, this paper describes the construction and expression of several novel human α7-ECD mutants with improved characteristics. The best of these, mut10, was found to have correct folding, a probably pentameric assembly and significantly enhanced solubility and ligand-binding properties compared to the wild-type and other mutants. All these properties, combined with its increased expression yield, suggest that mut10, in both its glycosylated and deglycosylated forms, is a promising starting material for structural studies on the human α7-nAChR-ECD, essential for the rational drug design to treat diseases related to α7-nAChR.

Acknowledgements

We are grateful to Dr Nigel Unwin for help with the electron microscopy. Special thanks are due to Dr Alexandros Sotiriadis for providing the muscle β1-ECD and data on deglycosylated mut10, Kalliopi Bitzopoulou for the muscle γ-ECD and Nikos Trakas and Anna Kokla for excellent technical support. This work was supported by a PENED grant (co-financed 80% by the EU-European Social Fund and 20% by the Greek Ministry of Development-GSRT) and by the EC FP7 project NeuroCypres (no. 202088).

MZ would like to dedicate his contribution to this work in memory of his beloved father, Stylianos Zouridakis.

Appendix A. Supplementary data

Supplementary data associated with this article can be found, in the online version, at doi:10.1016/j.bbapap.2008.11.002.

References

[1] J.P. Changeux, S.J. Edelstein, Nicotinic Acetylcholine Receptors, Odile Jacob, Paris, 2005, pp. 1–284.
[2] H.A. Lester, M.I. Dibas, D.S. Dahan, J.F. Leite, D.A. Dougherty, Cys-loop receptors: new twists and turns, Trends Neurosci. 27 (2004) 329–336.
[3] P.J. Corringer, N. Le Novere, J.P. Changeux, Nicotinic receptors at the amino acid level, Annu. Rev. Pharmacol. Toxicol. 40 (2000) 431–458.
[4] A. Karlin, Emerging structure of the nicotinic acetylcholine receptors, Nat. Rev. Neurosci. 3 (2002) 102–114.
[5] D. Kalamida, K. Poulas, V. Avramopoulou, E. Fostieri, G. Lagoumintzis, K. Lazaridis, A. Sideri, M. Zouridakis, S.J. Tzartos, Muscle and neuronal nicotinic acetylcholine receptors. Structure, function and pathogenicity, FEBS J. 274 (2007) 3799–3845.
[6] K. Brejc, W.J. van Dijk, R.V. Klaassen, M. Schuurmans, J. van Der Oost, A.B. Smit, T.K. Sixma, Crystal structure of an ACh-binding protein reveals the ligand-binding domain of nicotinic receptors, Nature 411 (2001) 269–276.
[7] P.H. Celie, S.E. van Rossum-Fikkert, W.J. van Dijk, K. Brejc, A.B. Smit, T.K. Sixma, Nicotine and carbamylcholine binding to nicotinic acetylcholine receptors as studied in AChBP crystal structures, Neuron 41 (2004) 907–914.
[8] P.H. Celie, I.E. Kasheverov, D.Y. Mordvintsev, R.C. Hogg, P. van Nierop, R. van Elk, S.E. van Rossum-Fikkert, M.N. Zhmak, D. Bertrand, V. Tsetlin, T.K. Sixma, A.B. Smit, Crystal structure of nicotinic acetylcholine receptor homolog AChBP in complex with an alpha-conotoxin PnIA variant, Nat. Struct. Mol. Biol. 12 (2005) 582–588.
[9] P.H. Celie, R.V. Klaassen, S.E. van Rossum-Fikkert, R. van Elk, P. van Nierop, A.B. Smit, T.K. Sixma, Crystal structure of acetylcholine-binding protein from *Bulinus truncatus* reveals the conserved structural scaffold and sites of variation in nicotinic acetylcholine receptors, J. Biol. Chem. 280 (2005) 26457–26466.
[10] C. Ulens, R.C. Hogg, P.H. Celie, D. Bertrand, V. Tsetlin, A.B. Smit, T.K. Sixma, Structural determinants of selective alpha-conotoxin binding to a nicotinic acetylcholine receptor homolog AChBP, Proc. Natl. Acad. Sci. U.S.A. 103 (2006) 3615–3620.
[11] S.B. Hansen, G. Sulzenbacher, T. Huxford, P. Marchot, P. Taylor, Y. Bourne, Structures of aplysia AChBP complexes with nicotinic agonists and antagonists reveal distinctive binding interfaces and conformations, EMBO J. 24 (2005) 3635–3646.
[12] Y. Bourne, T.T. Talley, S.B. Hansen, P. Taylor, P. Marchot, Crystal structure of a Cbtx–AChBP complex reveals essential interactions between snake alpha-neurotoxins and nicotinic receptors, EMBO J. 24 (2005) 1512–1522.
[13] S. Dutertre, C. Ulens, R. Buttner, A. Fish, R. van Elk, Y. Kendel, G. Hopping, P.F. Alewood, C. Schroeder, A. Nicke, A.B. Smit, T.K. Sixma, R.J. Lewis, AChBP-targeted alpha-conotoxin correlates distinct binding orientations with nAChR subtype selectivity, EMBO J. 26 (2007) 3858–3867.
[14] N. Unwin, Refined structure of the nicotinic acetylcholine receptor at 4 Å resolution, J. Mol. Biol. 346 (2005) 967–989.
[15] C.D. Dellisanti, Y. Yao, J.C. Stroud, Z.Z. Wang, L. Chen, Crystal structure of the extracellular domain of nAChR alpha1 bound to alpha-bungarotoxin at 1.94 Å resolution, Nat. Neurosci. 10 (2007) 953–962.
[16] S.J. Tzartos, T. Barkas, M.T. Cung, A. Mamalaki, M. Marraud, P. Orlewski, D. Papanastasiou, C. Sakarellos, M. Sakarellos-Daitsiotis, P. Tsantili, V. Tsikaris, Anatomy of the antigenic structure of a large membrane autoantigen, the muscle-type nicotinic acetylcholine receptor, Immunol. Rev. 163 (1998) 89–120.
[17] R.J. Hilf, R. Dutzler, X-ray structure of a prokaryotic pentameric ligand-gated ion channel, Nature 452 (2008) 375–379.
[18] C. Gotti, F. Clementi, Neuronal nicotinic receptors: from structure to pathology, Prog. Neurobiol. 74 (2004) 363–396.
[19] V. Avramopoulou, A. Mamalaki, S.J. Tzartos, Soluble, oligomeric, and ligand-binding extracellular domain of the human alpha7 acetylcholine receptor expressed in yeast: replacement of the hydrophobic cysteine loop by the

hydrophilic loop of the ACh-binding protein enhances protein solubility, J. Biol. Chem. 279 (2004) 38287–38293.
[20] J.D. Thompson, D.G. Higgins, T.J. Gibson, CLUSTAL W: improving the sensitivity of progressive multiple sequence alignment through sequence weighting, position-specific gap penalties and weight matrix choice, Nucleic Acids Res. 22 (1994) 4673–4680.
[21] A. Sali, T.L. Blundell, Comparative protein modelling by satisfaction of spatial restraints, J. Mol. Biol. 234 (1993) 779–815.
[22] B. Brooks, M. Karplus, Harmonic dynamics of proteins: normal modes and fluctuations in bovine pancreatic trypsin inhibitor, Proc. Natl. Acad. Sci. U. S. A. 80 (1983) 6571–6575.
[23] Y. Cheng, W.H. Prusoff, Relationship between the inhibition constant (K_1) and the concentration of inhibitor which causes 50 percent inhibition (I50) of an enzymatic reaction, Biochem. Pharmacol. 22 (1973) 3099–3108.
[24] N. Sreerama, R.W. Woody, Estimation of protein secondary structure from circular dichroism spectra: comparison of CONTIN, SELCON, and CDSSTR methods with an expanded reference set, Anal. Biochem. 287 (2000) 252–260.
[25] S.M. Kelly, T.J. Jess, N.C. Price, How to study proteins by circular dichroism, Biochim. Biophys. Acta 1751 (2005) 119–139.
[26] K. Kostelidou, N. Trakas, M. Zouridakis, K. Bitzopoulou, A. Sotiriadis, I. Gavra, S.J. Tzartos, Expression and characterization of soluble forms of the extracellular domains of the beta, gamma and epsilon subunits of the human muscle acetylcholine receptor, FEBS J. 273 (2006) 3557–3568.
[27] C. Toyoshima, N. Unwin, Three-dimensional structure of the acetylcholine receptor by cryoelectron microscopy and helical image reconstruction, J. Cell. Biol. 111 (1990) 2623–2635.
[28] M.L. Tierney, N. Unwin, Electron microscopic evidence for the assembly of soluble pentameric extracellular domains of the nicotinic acetylcholine receptor, J. Mol. Biol. 303 (2000) 185–196.
[29] S.B. Hansen, Z. Radic, T.T. Talley, B.E. Molles, T. Deerinck, I. Tsigelny, P. Taylor, Tryptophan fluorescence reveals conformational changes in the acetylcholine binding protein, J. Biol. Chem. 277 (2002) 41299–41302.
[30] G.B. Wells, R. Anand, F. Wang, J. Lindstrom, Water-soluble nicotinic acetylcholine receptor formed by alpha7 subunit extracellular domains, J. Biol. Chem. 273 (1998) 964–973.
[31] R. Anand, X. Peng, J. Lindstrom, Homomeric and native alpha 7 acetylcholine receptors exhibit remarkably similar but non-identical pharmacological properties, suggesting that the native receptor is a heteromeric protein complex, FEBS Lett. 327 (1993) 241–246.
[32] M. Zouridakis, K. Kostelidou, A. Sotiriadis, C. Stergiou, E. Eliopoulos, K. Poulas, S.J. Tzartos, Circular dichroism studies of extracellular domains of human nicotinic acetylcholine receptors provide an insight into their structure, Int. J. Biol. Macromol. 41 (2007) 423–429.
[33] A.B. Smit, K. Brejc, N. Syed, T.K. Sixma, Structure and function of AChBP, homologue of the ligand-binding domain of the nicotinic acetylcholine receptor, Ann. N.Y. Acad. Sci. 998 (2003) 81–92.
[34] M. Konstantakaki, S.J. Tzartos, K. Poulas, E. Eliopoulos, Model of the extracellular domain of the human alpha7 nAChR based on the crystal structure of the mouse alpha1 nAChR extracellular domain, J. Mol. Graph. Model 26 (2008) 1333–1337.
[35] W.L. DeLano, The PyMOL Molecular Graphics System on World Wide Web (2004) http://www.pymol.org.